Materials Science & Engineering A 622 (2015) 168–177

Contents lists available at ScienceDirect

Materials Science & Engineering A

journal homepage: www.elsevier.com/locate/msea

Interfacial study of NiTi–Ti_3SiC_2 solid state diffusion bonded joints

A. Kothalkar [a], A. Cerit [b], G. Proust [c], S. Basu [d], M. Radovic [a,*], I. Karaman [a,*]

[a] Department of Materials Science and Engineering, Texas A&M University, College Station, TX 77843, USA
[b] Department of Industrial Design Engineering, Erciyes University, Kayseri, Turkey
[c] School of Civil Engineering, University of Sydney, Sydney, NSW 2006, Australia
[d] Agilent Technologies, Chandler, AZ, USA

ARTICLE INFO

Article history:
Received 20 July 2014
Received in revised form
6 October 2014
Accepted 13 October 2014
Available online 4 November 2014

Keywords:
Ti_3SiC_2
NiTi
Shape memory alloys
MAX phases
Solid state diffusion bonding

ABSTRACT

The interfaces between the stress-assisted diffusion bonded Ti_3SiC_2 and equiatomic NiTi, two distinct material systems that show pseudoelasticity were studied. The interfaces were formed in the 800–1000 °C temperature range, for 1, 5 and 10 h under flowing argon. Bonding was observed in all the cases considered, except at 800 °C after 1 h. Morphology and reaction phases in the interface were characterized using scanning electron microscopy, elemental micro probe analysis and electron back-scatter diffraction analysis. The interfacial structure formed between NiTi and Ti_3SiC_2 layers consists of NiTi/Ti_2Ni/Ti_5Si_3/NiTiSi/Ti_3SiC_2. Diffusion of Si into NiTi from Ti_3SiC_2, and Ni from NiTi into reaction zone was found to be responsible for the formation of reaction layers in the interface and thus for bonding at these conditions. The overall reaction layer thickness grows following the parabolic kinetic law. Nano-indentation and Vickers micro hardness tests were carried out to investigate the mechanical properties of the interface. Nano-indentation showed that the elastic moduli of the phases in the interface are close to that of Ti_3SiC_2 while their hardness is higher than that of both Ti_3SiC_2 and NiTi. Artificially formed cracks through microindents were observed to be branched and propagated into Ti_3SiC_2 phase indicating good resistance against delamination.

1. Introduction

Ti_3SiC_2 belongs to the family of nanolayered ternary ceramics having a general formula $M_{n+1}AX_n$ (MAX) where $n=1$, 2, or 3; M is an early transition metal; A is an A-group element (a subset of group 13–16 elements); and X is C and/or N [1,2]. The MAX phases have attracted attention due to their unusual and unique combination of metallic and ceramic properties, in other words, they are stiff but readily machinable ceramics, with excellent thermal and electrical conductivity and low coefficient of thermal expansion. They are also thermal shock resistant and damage tolerant, while some of them possess good oxidation, fatigue and corrosion resistance [1–4]. Among all the MAX phases known to date, Ti_3SiC_2 is the most characterized MAX phase. Like other MAX phases, Ti_3SiC_2 shows spontaneous fully reversible, strain rate independent hysteretic stress–strain loops when cyclically loaded in compression [5] or tension [6]. Thus, a significant portion of the mechanical energy – about 25% at 1 GPa in the case of Ti_3SiC_2 – can be dissipated during each cycle [7]. At this time, Incipient Kink Bands (IKBs) that form during loading and annihilate during unloading are believed to account for this unusual hysteretic (or pseudoelastic) effect. Above brittle-to-plastic transition temperature, i.e. above 1000–1100 °C, stress–strain response of Ti_3SiC_2 becomes a strong function of temperature and deformation rate, and it can be plastically deformed to strains exceeding 25% even in tension [6,8,9].

Because of the unusual and unique combination of properties that are uncommon for most ceramics, Ti_3SiC_2 have been examined as a ceramic reinforcing phase in several different metal–ceramic composites [10–15], or as protective coating for metallic alloys [3]. Recently, few investigations have focused on studying the processing, thermo-mechanical characterization and damping behavior of NiTi–MAX phase composites that combine two unique material systems demonstrating different pseudoelastic mechanisms [16,17]. NiTi is a benchmark Shape Memory Alloy (SMA) that has been used for various applications in medical industry [18] and different engineering fields [19] because of its excellent shape memory performance combined with good ductility, strength, corrosion resistance and damping capability. NiTi shows thermoelastic martensitic phase transformation from a monoclinic, B19′, martensite (low temperature) phase to a cubic, B2, austenite (high temperature) phase upon heating past a particular temperature (Austenite finish, A_f). As a result of reversible thermoelastic phase transformation, NiTi shows not only shape memory effect, in which original shape before mechanical deformation can be

* Corresponding authors.
E-mail addresses: mradovic@tamu.edu (M. Radovic), ikaraman@tamu.edu (I. Karaman).

http://dx.doi.org/10.1016/j.msea.2014.10.033
0921-5093/

restored by heating previously deformed phase, but also pseudoelasticity during isothermal application of mechanical load above A_f temperature [20].

Recently processed and characterized NiTi–Ti_3SiC_2 composites demonstrate higher damping capacity than any of the metal/MAX composites reported in the literature to date, up to 200 MPa stress levels [16]. Thermo-mechanical cycling (i.e. training) in these composites leads to further increase in damping levels and introduction of residual stresses, which are evident in the observed two way shape memory behavior of the composites. An effort has also been made recently to model SMA–MAX phase system by finite element modeling constructed using a 3D image based technique utilizing X-ray micro tomography to investigate the evolution of residual stresses during thermo-mechanical cycling of the composites [21]. The biggest challenge in fabricating these composites lies in controlling and reducing reactions between NiTi and MAX phases during co-sintering NiTi and MAX phase powders in 960–1000 °C temperature range [16,17]. The latter is important for two reasons. First, it is crucial to preserve the chemistry of NiTi during processing because the capability of controlling residual stresses in the composite and high mechanical damping during cyclic loading depends on the percent of the phase transformable NiTi in the composite. Second, severe chemical reactions between NiTi and MAX phases during processing of the composite can introduce complex multiphase interfaces that can in turn have more dominant role in determining the overall properties of the metal/ceramic composite than its constituents.

As Ti_3SiC_2 and similarly other structural materials need to be joined with each other, it is important to investigate the feasibility of joining SMAs with these materials. Apart from its current applications, many more potential applications can be realized by successful joining of SMAs to other materials systems. For example, joining of NiTi to aerospace grade alloys such as Ti–6Al–4V could lead to its use as an adaptive serrated nozzle, thus providing the highly desired noise reduction for the aerospace industry [23]. Similarly, its successful joining to stainless steel could increase its range of applications [24]. Various attempts have been made to join NiTi with other material systems using joining techniques such as friction welding [25], laser welding [23,24,26–28] and femtosecond laser irradiation [29].

The objective of this study is therefore to investigate the formation and evolution of microstructures in the diffusion bonded NiTi–Ti_3SiC_2 interface at elevated temperatures. Previously, pressureless diffusion bonding of NiTi with Ti_3SiC_2 was studied only in the 1000–1300 °C temperature range [22] where no bonding was observed at 1000 °C, while relatively thick (45–55 μm) interfacial reaction layers were observed in the range at 1100–1200 °C. Therein [22], the formation of the interfacial reaction layers is attributed to Si diffusion from Ti_3SiC_2 into NiTi assisted by the liquid phase diffusion in the interface. In the current study, the feasibility of joining bulk NiTi and Ti_3SiC_2 components using solid state diffusion bonding mechanism in the temperature range of 800–1000 °C is investigated. Through the investigations of the phases in the interface and their microstructures, the reaction mechanisms and growth kinetics of the reaction layer during pressure-assisted diffusion bonding have been derived at the conditions that are close to those used in NiTi–Ti_3SiC_2 composite processing [16,17]. Furthermore, one of the goals of this study is to evaluate the mechanical properties of the NiTi–Ti_3SiC_2 interface, because load transfer across the interfaces between metal and ceramic components plays an important role in determining the overall mechanical properties of the composites [30]. Lastly, this study also provides basis for understanding the reactivity of Ti_3SiC_2 with NiTi at elevated temperatures and designing and controlling the microstructures of NiTi–Ti_3SiC_2 joints and composites.

2. Experimental procedures

Bulk equiatomic NiTi having transformation temperatures of 45, 61, 76 and 94 °C for martensite finish (M_f), martensite start (M_s), austenite start (A_s), and austenite finish (A_f) respectively, was acquired from SAES Getters in cold drawn condition. Bulk Ti_3SiC_2 samples were reaction sintered from Ti, SiC and C powder mixtures at 1400 °C, for 8 h using hot isostatic pressing. The NiTi and Ti_3SiC_2 samples were cut using wire electrical discharge machining (EDM) to the sizes of $10 \times 5 \times 2$ mm^3. These samples were surface grinded to remove the EDM layer, followed by mechanical polishing prior to joining. A customized loading fixture of rectangular alumina plates with one hole at each corner along with appropriate alumina screws and bolts was prepared to hold both the NiTi and Ti_3SiC_2 samples on top of each other during bonding at joining temperatures. At room temperature, the whole fixture with samples between them was compressed to a uniaxial stress of 150 MPa and unloaded to 20 MPa in an MTS Insight electromechanical test frame. Holding the load that corresponds to stress at 20 MPa, the bolts were tightened in the fixture and the load was removed afterwards. The objective of initial pre-loading was to achieve good, intimate contact between the mating surfaces. The fixture was then placed in an alumina boat in the tube furnace (MTI Corporation, Model GSL 1600X) to carry out bonding experiments. Previously, successful joining of these two materials has been achieved by liquid state diffusion bonding at 1100 and 1200 °C with 45–55 μm thick interface reaction layers [22]. In this study, the temperature range of 800–1000 °C was selected to investigate whether solid state diffusion bonding could be used to join NiTi–Ti_3SiC_2 couples and to determine the kinetics of the process. The vacuum level in the tube furnace was held at 2×10^{-2} Pa for 5 min followed by purging with ultra-high purity Argon. The purging process was repeated once again before heating the samples to desired temperatures in flowing argon environment as it is important to have an oxygen free atmosphere to prevent the formation and growth of oxide films. The presence of oxide layer on either of the mating surfaces can prevent their contact and thus degrade the kinetics of interface creation by hindering the diffusion [31]. Heating/cooling rate of 5 °C/min was used during bonding experiments in the tube furnace.

The cross-sections of the bonded NiTi–Ti_3SiC_2 samples were cut using a low speed diamond saw before mounting in epoxy, and polished using standard metallographic procedures up to final step of polishing with 1 μm diamond paste followed by ultrasonic cleaning in ethanol. The microstructures of the interfaces were characterized using a field emission scanning electron microscope (FE – SEM, Quanta 600 FEG, FEI, Oregon, USA). Electron micro probe analysis (EPMA) was used for quantitative analysis of different phases in the interface, through the spot analysis. An excitation voltage of 15 keV and a beam current of 10 nA was used in the spot analysis. Energy dispersive spectroscopy (EDS) line scan was also carried out to determine the elemental distribution across the interface.

Electron backscattered diffraction (EBSD) was used to determine the reaction phases in the interface. An additional polishing step using a 0.05 μm colloidal silica solution was necessary for the EBSD characterization. The SEM used for the characterization was a Zeiss Ultra Plus FEGSEM, equipped with an Oxford Instrument AZtec EDS and Electron Backscatter Diffraction (EBSD) system and a Nordlys nano EBSD detector. The accelerating voltage was set at 20 keV and the working distance was between 10 and 12 mm. The step size used to scan the area of interest was 50 nm.

The nano-indentation measurements across the NiTi–Ti_3SiC_2 interface were conducted using an Agilent Technologies G200 Nanoindenter and a diamond Berkovich indenter tip. A maximum penetration depth of 250 nm was used for all the indents. An array

of indents was made to map the elastic modulus and hardness of different phases in and around the NiTi–Ti_3SiC_2 interface.

Vickers micro-hardness tests were also carried out across the interface for qualitative analysis. A series of indentation loads (0.1, 0.2, 0.3 and 0.5 kg) were applied to obtain indents on the interface using diamond pyramidal indenter. For each indent, a dwelling time of 13 s at peak load was used. After the hardness tests, SEM was used to observe the indentations and regions around them. Both the nano-indentation and Vickers micro-hardness tests were conducted at ambient temperature where NiTi is in fully martensite phase.

3. Results and discussion

3.1. Microstructure of the bonded NiTi–Ti_3SiC_2 interface

Fig. 1 shows the cross sectional views of the microstructure of NiTi–Ti_3SiC_2 interface after diffusion bonding at 800, 900 and 1000 °C for 1, 5 and 10 h. All the microstructural images are shown on the *X*–*Y* plot where the *X*-axis is the bonding time and the *Y*-axis is the bonding temperature. In all the micrographs in Fig. 1, the lighter region on the left is equiatomic NiTi and the dark gray region on the right is Ti_3SiC_2. In between the two, the interface is

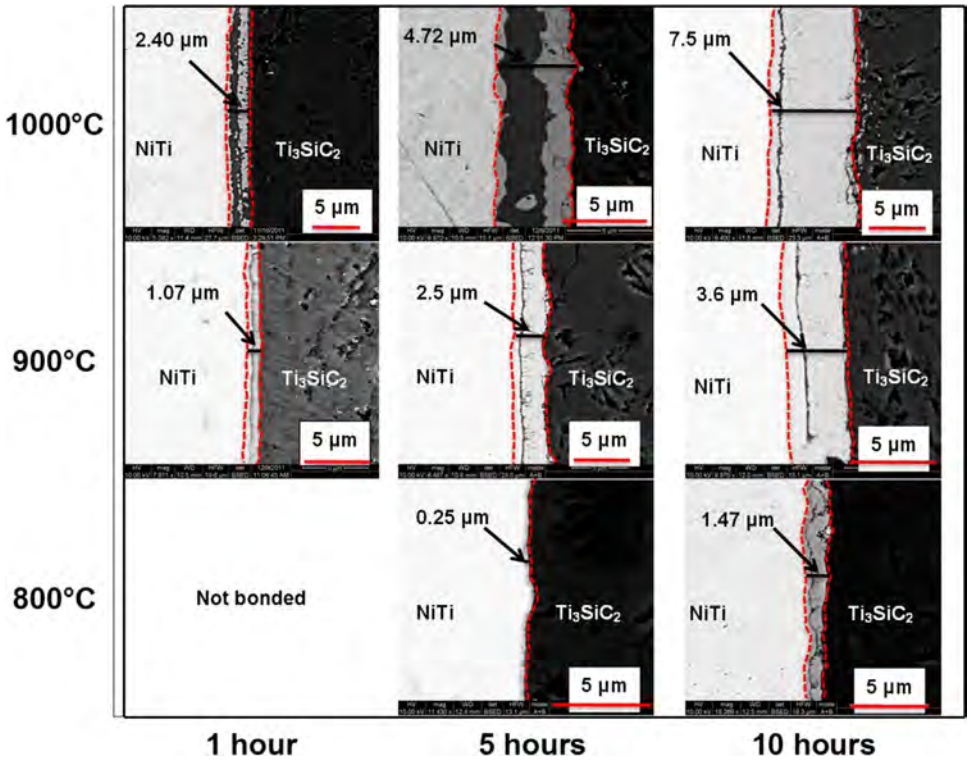

Fig. 1. Microstructural evolution of the NiTi–Ti_3SiC_2 interface with time and temperature obtained by SEM. Dotted (red) line indicates the start and end of the interface region between NiTi and Ti_3SiC_2. The numbers shown in each of the micrographs are the thicknesses of the interface as indicated by the black horizontal lines on each image in the interface region. (For interpretation of the references to color in this figure legend, the reader is referred to the web version of this article.)

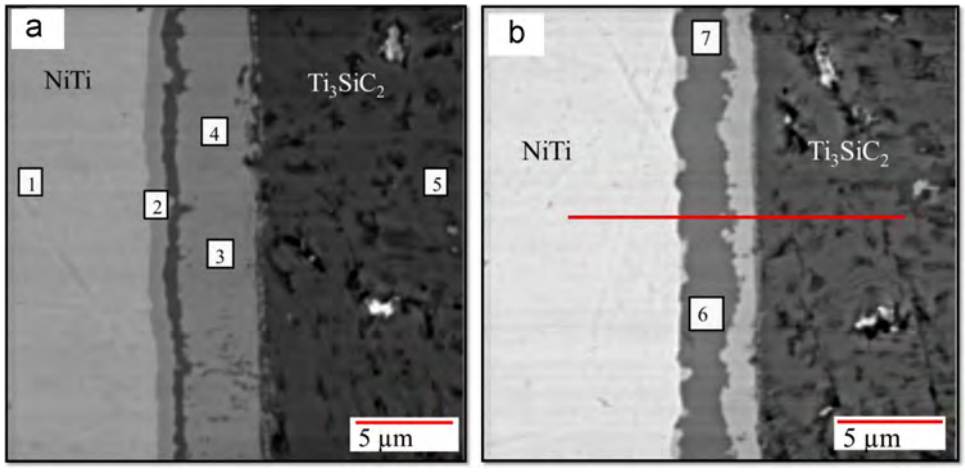

Fig. 2. Back-scattered electron images of the NiTi–Ti_3SiC_2 interface for the bonding condition of 1000 °C, 5 h. Points 1–5 in (a) and 6–7 on (b) show the location where quantitative spot spectra are obtained by electron microprobe for determining the composition of different reaction phases formed in the interface. Table 1 lists the composition of all the points shown in this figure. Points 1 and 5 are 10 μm away from the interface in the NiTi and Ti_3SiC_2 regions, respectively. The horizontal red line in (b) indicates the location of the line scan shown in Fig. 4. (For interpretation of the references to color in this figure legend, the reader is referred to the web version of this article.)

marked with vertical dotted red lines to denote the start and end of the reaction layer in the interface. The numbers on each of the image are the lengths of the horizontal black lines which represents the average interface thickness. Evolution of the interface thickness with time at different temperatures along with the kinetics of the reaction will be described later (Section 3.3). As it can be seen in Fig. 1, bonding has been observed for all conditions except at 800 °C for 1 h. In our previous study, NiTi and Ti_3SiC_2 have been joined in the temperature range of 1100–1200 °C using pressureless liquid phase assisted diffusion bonding [22], however, no bonding was observed at 1000 °C, most likely due to poor contact between the two surfaces in the absence of any preloading stress.

As it can be seen in Figs. 1 and 2, at each bonding condition, formation of three distinct layers in the interface is observed. One light gray layer adjacent to NiTi and the other adjacent to Ti_3SiC_2. These two light gray layers are separated by a third dark gray layer in between. To determine theses reaction phases in the interface, EPMA was used. Fig. 2 shows the selected, but typical, back-scattered electron micrographs of the interface for the bonding condition of 1000 °C, 5 h. Points 1–5 in Fig. 2(a) and 6, 7 in (b) show the location where quantitative spot spectra is obtained by EPMA. Table 1 lists the atomic percentages of Si, Ni, Ti and C at the locations marked in Fig. 2. The percentage of C was calculated by taking the difference between the total (100%) and the sum of the measured atomic percentages of Si, Ni and Ti. Point 1 corresponds to equiatomic NiTi as ratio of Ni to Ti is almost 1:1 and point 5 to Ti_3SiC_2 as the ratio of Ti to Si is 3:1. Points 3 and 4 are on the same light gray phase adjacent to Ti_3SiC_2 and their compositions suggest it to be NiTiSi phase. Points 6 and 7 in Fig. 2(b) are on the dark gray phase which separates the two light gray phases in the interface. The compositions of these points suggest the phase to be Ti_5Si_3 with the ratio of Ti to Si being close to 5:3. Low Ni (around 1%) is also observed most likely due to scattering from adjacent Ni containing phases. Composition of point 2 in Fig. 2(a), which is located in light gray phase adjacent to NiTi, is slightly off from that of Ti_2Ni phase. This is due to the fact that its thickness is less than 1 μm and the beam from the microprobe scatters more than a micron during quantitative analysis, thereby detecting extra Ni from the adjacent NiTi phase. All the probable phases (Ti_2Ni, Ti_5Si_3 and NiTiSi) in the interface are also present in the ternary phase diagrams of Ni, Ti and Si at 900 [32] and 1000 °C [33], as shown schematically in Fig. 3 following the phase diagram at 1000 °C [33]. All the three phases observed in the interface form continuous layers as shown in Fig. 2(a) whereas in (b), the light gray phase (Ti_2Ni) closer to NiTi is discontinuous. Both the images are obtained for the same condition of 1000 °C, 5 h. Also the micrograph shown in Fig. 1 for 1000 °C, 5 h is similar to the one in Fig. 2(b). The most probable reason for the observed difference is the amount of local pressure experienced in these locations in the diffusion couple is different possibly due to surface asperities.

Table 1
Atomic percentages of Si, Ni and Ti from electron microprobe spot analysis of the different points marked in Fig. 2 and also the probable phases for each location in the interface. BDL means below detection limit, which was 0.2% for Ni.

Location (Fig. 2)	Atomic%				Probable phase
	Si	Ni	Ti	C	
1	0.2	49.2	50.6	0	NiTi
2	6.3	35.4	58.3	0	Ti_2Ni
3	31.6	29.8	33.5	5.1	NiTiSi
4	31.2	29.5	33.5	5.8	NiTiSi
5	16.8	BDL	51.8	31.4	Ti_3SiC_2
6	36.0	1.2	62.8	0	Ti_5Si_3
7	35.4	1.8	62.8	0	Ti_5Si_3

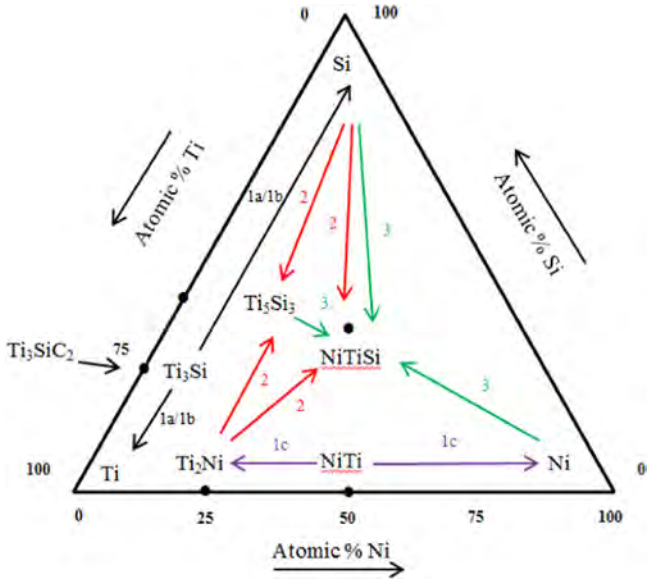

Fig. 3. Schematic of the Ni–Ti–Si ternary phase diagram at 1000 °C following [33], showing the phases observed at interface after the 1000 °C, 10 h bonding. The numbers labeled 1 (a/b, black), 1 (c, purple), 2 (red) and 3 (green) on the schematic correspond to the equations shown in the text. (For interpretation of the references to color in this figure legend, the reader is referred to the web version of this article.)

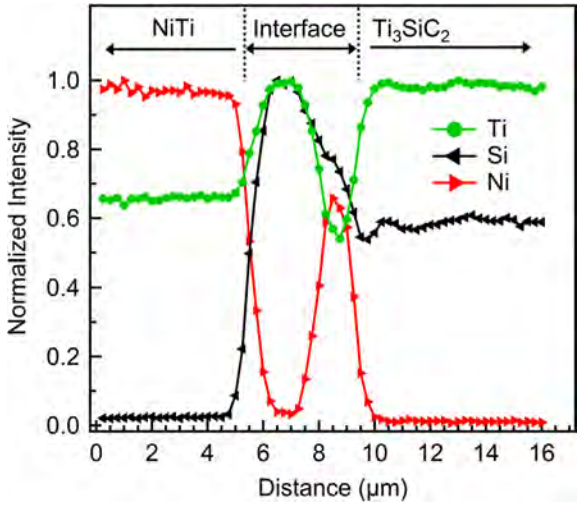

Fig. 4. Line scan for Ni (red), Si (black) and Ti (green) across the NiTi–Ti_3SiC_2 interface for the bonding condition of 1000 °C, 5 h indicated in Fig. 2(b) with a horizontal (red) line. (For interpretation of the references to color in this figure legend, the reader is referred to the web version of this article.)

Elemental distribution of Ni, Si and Ti across the interface determined using the EDS line scan analysis for the bonding condition of 1000 °C, 5 h is shown in Fig. 4. The horizontal line (red) marked in the Fig. 2(b) shows the location of the line scan across the interface. For each element, the normalized intensity is obtained by dividing the intensity at each point with the maximum intensity. Three regions, NiTi, interface and Ti_3SiC_2 are clearly marked on the line scan. Very low intensities of Si and Ni are observed in NiTi and Ti_3SiC_2 regions respectively suggesting minor diffusion of Si and Ni away from the interface. At the NiTi side of the interface region, the intensity of Ni first drops to near zero and then locally increases before going down again. The region without Ni in the interface corresponds to Ti_5Si_3 phase where only Ti and Si elements are detected. When the Ni intensity reaches a local maximum before dropping to near zero, Ti and Si elements are also detected and this region in the interface

adjacent to Ti_3SiC_2 corresponds the NiTiSi phase. Thus, the line scan is consistent with the results shown in Table 1 and Fig. 2(b).

3.2. Electron backscatter diffraction (EBSD) observations and reaction mechanisms

Figs. 5 and 6 show the distribution of different phases in the NiTi–Ti_3SiC_2 interface for the conditions of 900 °C, 5 h and 1000 °C, 10 h, respectively, obtained using EBSD analysis. EBSD analysis confirmed and substantiated the formation of Ti_2Ni, Ti_5Si_3 and NiTiSi reaction phases in the interface, earlier inferred from the results of quantitative analysis and Ni–Ti–Si ternary phase diagram [33], schematically shown in Fig. 3. Fig. 5(a) shows the back-scattered electron image of the NiTi–Ti_3SiC_2 interface formed at 900 °C, 5 h, marked with area A from where the phase map shown in Fig. 5(b) is obtained using EBSD. Clearly, the interface has a structure of NiTi/Ti_2Ni/Ti_5Si_3/NiTiSi/Ti_3SiC_2. A similar interface structure is observed in Fig. 6 wherein all the reaction phases form continuous layers in the interface at 1000 °C, 10 h. TiC phases are detected in the Ti_3SiC_2 phase and also along the boundary between NiTiSi and Ti_3SiC_2. Small amount of TiC is expected to form as a result of Si de-intercalation and as Ti_3SiC_2 phase usually

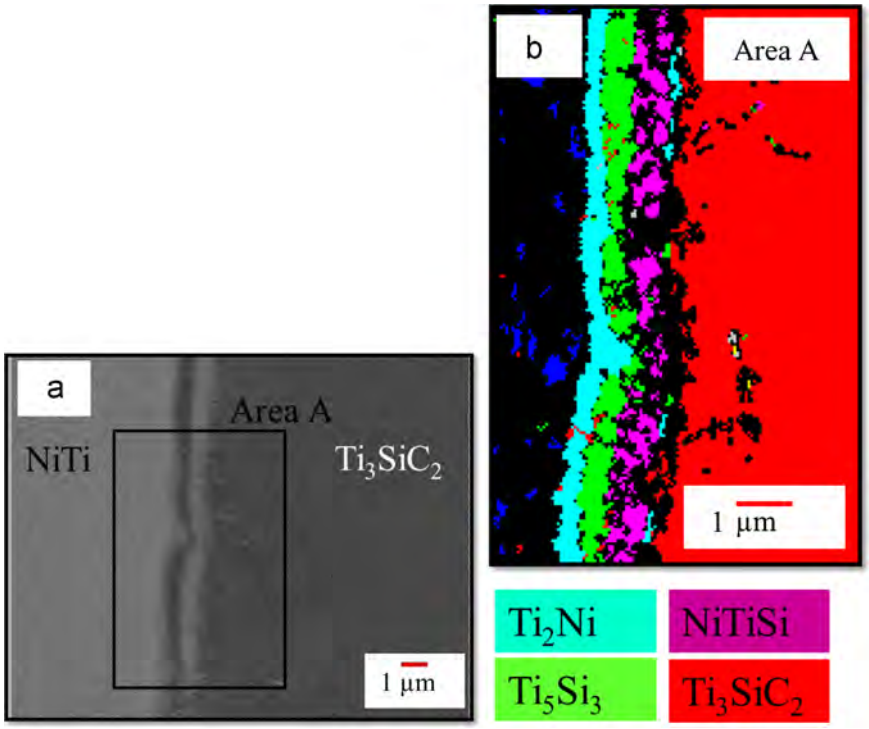

Fig. 5. Images of the NiTi–Ti_3SiC_2 interface for the bonding condition of 900 °C, 5 h (a) BSE image, and (b) Electron backscattered diffraction (EBSD) phase map of the "Area A" marked in (a) showing the distribution of the reaction phases, NiTiSi (pink), Ti_5Si_3 (green) and Ti_2Ni (light blue) in the interface. The MAX phase is indicated in red and the blue areas are the NiTi phase that could be indexed. The black areas in the map represent areas where diffraction patterns could not be obtained due to sample preparation issues or resolution limit of the technique (this second explanation is especially true for the NiTi phase that its martensite phase consists of very thin needles). (For interpretation of the references to color in this figure legend, the reader is referred to the web version of this article.)

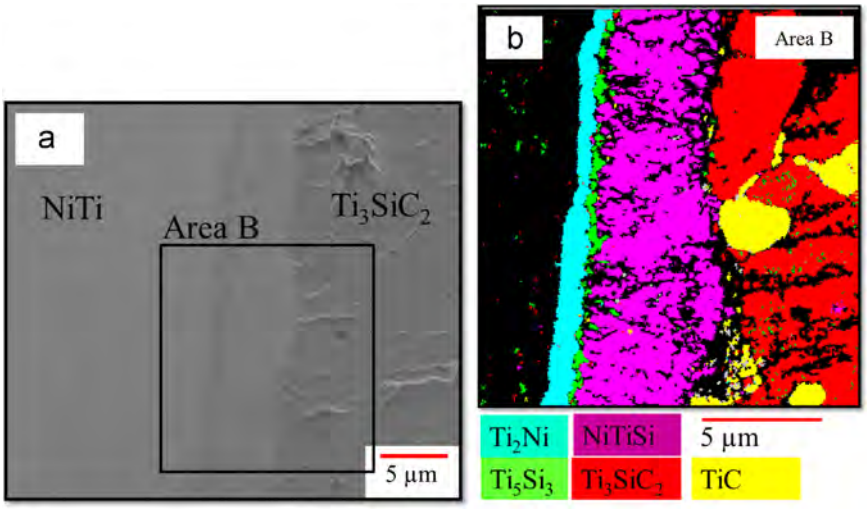

Fig. 6. Images of the NiTi–Ti_3SiC_2 interface for the bonding condition of 1000 °C, 10 h (a) BSE image, and (b) Electron backscattered diffraction (EBSD) phase map of the area B marked in (a) showing the distribution of the reaction phases, Ti_2Ni (light blue), Ti_5Si_3 (green) and NiTiSi (pink). Also shown are TiC (yellow) and Ti_3SiC_2 (red). (For interpretation of the references to color in this figure legend, the reader is referred to the web version of this article.)

contains few percent impurities in the form of TiC. From the combined results of EBSD, quantitative EPMA analysis, micrographs of the microstructures of the NiTi–Ti_3SiC_2 interface at various bonding conditions, and the ternary phase diagram, a reaction mechanism has been proposed as described in the Eqs. (1)–(3)

$$Ti_3SiC_2 \rightarrow xSi + Ti_3Si_{1-x}C_2 \quad (1a)$$

$$4Ti_3SiC_2 \rightarrow Si + Ti_5Si_3C_y + 7TiC_{1-x} \quad \text{where } y = 1 + 7x \quad (1b)$$

$$2NiTi \rightarrow Ni + Ti_2Ni \quad (1c)$$

$$5Ti_2Ni + 8Si \rightarrow Ti_5Si_3 + 5NiTiSi \quad (2)$$

$$Ti_5Si_3 + 5Ni + 2Si \rightarrow 5NiTiSi \quad (3)$$

As "A" element is the most weakly bonded element in the MAX phase [34], the decomposition of Ti_3SiC_2 by de-intercalation of Si may lead to the formation of non-stoichiometric $Ti_3Si_{1-x}C_2$ as per Eq. (1a), whereas formation of $Ti_5Si_3C_y$ and non-stoichiometric TiC_{1-x} phase may occur on further decomposition of Ti_3SiC_2, where $y=1+7x$, according to Eq. (1b). The reaction (Eq. (1b)) has been previously observed when bulk NiTi and Ti_3SiC_2 are diffusion bonded at 1100 °C [22]. Various researchers have studied the reactions and stability of MAX phases in the presence of metals and alloys at elevated temperatures [22,35–42]. Gu et al. [35] studied the reactions between Ti and Ti_3SiC_2 in the temperature range of 1000–1300 °C and found out that de-intercalation of Si is one of the ways that leads to the decomposition of Ti_3SiC_2. In this study, on the other side of the interface, Ni from NiTi diffuses out leaving behind a Ti-rich Ti_2Ni phase according to Eq. (1c). Yin et al. [40] studied the microstructure and diffusion bonding of Ni–Ti_3SiC_2 joints and found out that diffusion of Ni towards the reaction zone is the main controlling step in the bonding process. Here, Eqs. (1a)–(1c) occur simultaneously followed by the combination of Si from Ti_3SiC_2 with the Ti-rich Ti_2Ni phase to form Ti_5Si_3 and NiTiSi phase according to Eq. (2). Ni coming out of NiTi as per Eq. (1c) gets consumed by reacting with Ti_5Si_3 formed as per Eq. (2), and Si diffusing through NiTiSi phase, leading to the formation of more NiTiSi phase according to Eq. (3). On further increasing the time, more Ti_2Ni phase is formed which gets consumed in forming Ti_5Si_3 and NiTiSi phases. However, Ti_5Si_3 also gets consumed by Ni and Si to form NiTiSi phase. Thus, NiTiSi phase could be imagined to be moving towards NiTi formed by consuming Ti_2Ni phase and Ti_5Si_3 phase. Thus, arguably the most probable location of the original interface would lie between the current Ti_3SiC_2 and NiTiSi phases. At 1000 °C, 10 h, TiC phase is also observed due to possible complete loss of Si from Ti_3SiC_2 phase at higher temperatures and longer time compared to other bonding conditions. The presence of intermetallic phases such as Ti_5Si_3, Ti_2Ni and NiTiSi were also observed in the reaction layer formed between NiTi and Ti_3SiC_2 composites sintered at 960 °C, for 8 min under 100 MPa uniaxial pressure using the spark plasma sintering (SPS) technique [17].

3.3. Bonding kinetics

From the results of quantitative analysis using EPMA and EBSD, the presence of Ti_2Ni, Ti_5Si_3 and NiTiSi reaction phases in the NiTi–Ti_3SiC_2 interface is confirmed. The total thickness of the reaction layer which is a combination of all the three sublayers (Ti_2Ni, Ti_5Si_3 and NiTiSi rich sublayers) is measured at each bonding temperature and time using backscattered electron imaging. Total reaction layer thickness and standard deviations are calculated from an average of at least 15 measurements for each bonding condition. Fig. 7(a) shows the plot of total reaction layer thickness versus square root of the bonding time at 800, 900 and 1000 °C. At each

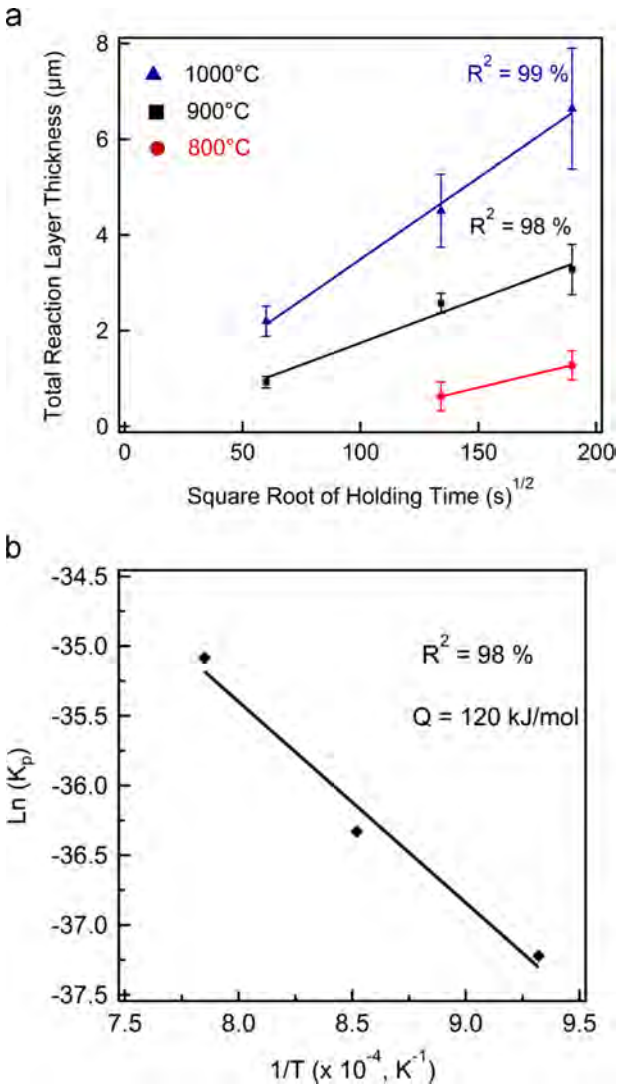

Fig. 7. (a) Evolution of the total reaction layer thickness with the square root of holding time at different temperatures for the NiTi–Ti_3SiC_2 interface, and (b) Arrhenius plot of the parabolic rate constant versus the reciprocal of the absolute bonding temperature in the temperature range of 800–1000 °C.

temperature, as the holding time is increased, the thickness of the total reaction layer also increases, while for the same holding time, the thickness increases as the holding temperature is increased. Good linear relationships are observed in Fig. 7(a), for all the temperatures wherein all the best fit lines have an R^2 value > 0.98 indicating that the growth of the reaction layer follows the parabolic kinetic law, i.e. $d^2 = 2K_p t$ where d is the total thickness of the reaction layer, K_p is the parabolic rate constant and t is the time. The total reaction layer thicknesses vary from less than a micron at 800 °C, 5 h to 7 μm at 1000 °C, 10 h bonding conditions. These layer thicknesses are an order of magnitude smaller when compared to the 45–55 μm reaction layers reported in the temperature range of 1100–1200 °C between NiTi and Ti_3SiC_2 diffusion couples [22]. The difference lies in the mechanism of diffusion bonding, liquid state diffusion bonding above 1000 °C [22] whereas solid state diffusion bonding below 1000 °C obtained here. The presence of liquid phase also leads to increased reaction and higher number of reaction phases present in the interface at 1100–1200 °C [22] as compared to those obtained in this study below 1000 °C.

Parabolic rate constant is obtained for each bonding temperature from the slopes of the curves shown in Fig. 7(a). However, one

needs to be careful while determining K_p from the slopes of the curves in Fig. 7, as the calculated K_p is for a combination of reactions given in Eqs. (1)–(3) and not for a single reaction. To obtain an approximate value for the activation energy of the overall bonding process, the K_p is plotted as a function of bonding temperature in the temperature range of 800–1000 °C. Fig. 7(b) indicates a good linear relationship with an R^2 value=0.98 between Ln (K_p) and the inverse of absolute temperature in accordance with the Arrhenius equation, $K_p = A \exp(-Q/RT)$ where A is the pre-exponent factor, Q is the bonding activation energy, R is the universal gas constant and T is the absolute temperature. Using the slope and the intercept of the straight line in Fig. 7(b), the bonding activation energy (Q) and the pre-exponent factor (A) are found to be 120 kJ/mol and 4.34×10^{-11} m^2/s, respectively. Thus the Arrhenius equation for the NiTi–Ti_3SiC_2 interface in the temperature range of 800–1000 °C can be written as

$$K_p = 4.34 \times 10^{-11} \exp\left(\frac{-120{,}000}{RT}\right) \mathrm{m^2/s} \quad (4)$$

For the Ni–Ti_3SiC_2 diffusion couple, the activation energy in the temperature range of 800–1100 °C is reported to be 118 kJ/mol [40], which is very close to the observed value of 120 kJ/mol between NiTi and Ti_3SiC_2 in the temperature range of 800–1000 °C. This substantiates the argument that Ni diffuses out from NiTi forming another intermetallic compound, Ti_2Ni, and behaves in a similar fashion as in the case of pure Ni–Ti_3SiC_2 diffusion couple. Activation energy values for other metal–Ti_3SiC_2 systems have also been reported in the literature: 156 kJ/mol for Ti–6Al–4V–Ti_3SiC_2 in the range of 1200–1300 °C [41] and 132 kJ/mol for Si–Ti_3SiC_2 in the range of 1200–1350 °C [42]. Therefore the value obtained here falls within the range of previously measured values for similar material couples.

3.4. Mechanical characterization

Mechanical characterization of the NiTi–Ti_3SiC_2 interface was done using nano-indentation and Vickers micro hardness tests. Here, nano-indentation is used to perform quantitative analysis and obtain hardness and elastic modulus values of the interface. Owing to the small size of the interfaces formed at these conditions, Vickers micro-hardness test was used as a qualitative tool to investigate crack initiation/propagation, if any, in and around the interface regions. Both tests were performed at room temperature where the NiTi is completely in the martensite phase.

3.4.1. Nano-indentation

Fig. 8(a) and (b) shows 3-D plots of the hardness and elastic modulus, respectively, obtained using nano-indentation across the NiTi–Ti_3SiC_2 interface for the bonding condition of 1000 °C, 5 h. A grid of 100 indents (10 × 10) each separated by a distance of 3 μm is made across the interface as shown in Fig. 8(c). Indents lie partially in NiTi, interface and Ti_3SiC_2. Hardness and elastic modulus are obtained for each indent using the Oliver–Pharr method [43]. Hardness of the reaction zone in the interface is higher than that observed for both NiTi and Ti_3SiC_2. An average hardness of 17.55 ± 0.95 GPa is obtained for the interface as compared to 5.44 ± 0.73 GPa for NiTi and 11.86 ± 1.80 GPa for Ti_3SiC_2. Elastic modulus of the reaction zone is higher than NiTi and close to that of Ti_3SiC_2. An average elastic modului of 278.68 ± 10.02 GPa is obtained for the interface as compared to 91.62 ± 11.16 GPa for NiTi and 263.21 ± 31.89 GPa for Ti_3SiC_2. Elastic moduli obtained for pure components are similar to the previously reported literature values for martensitic NiTi [44] and Ti_3SiC_2 [45,46] using nano-indentation. Most of the indents within the interface lie in the NiTiSi phase which is responsible for the increased hardness as compared to the individual components.

3.4.2. Vickers micro-hardness test

Vickers micro-hardness test is used on/near the NiTi–Ti_3SiC_2 interface to investigate whether any cracks initiate and/or propagate near the interface. Any further quantitative analysis of these results is difficult to perform as most of the indents are larger than the interface thickness for most of the bonding conditions. As the interface thickness is in the order of few microns compared to the indent size which is in the range of tens of microns, the indents lie partially in NiTi, interface and Ti_3SiC_2 regions. Interestingly for few cases, cracks near the NiTi–Ti_3SiC_2 interface are observed around the indents. One such indent obtained at a test load of 0.5 kg is shown in Fig. 9(a). No cracks are observed in the NiTi region whereas initiation of a single crack is observed at the bottom edge of the indent in the Ti_3SiC_2 regions close to the interface. This is expected as NiTi is known for its ductility and Ti_3SiC_2 for its high damage tolerance. In brittle solids, Vickers indentation leads to crack initiation at the corners of the indents [47]. However, for pure MAX phases, it is very difficult to induce cracking from the corners of the Vickers indents [48–50]. Rather, damage in the form of delaminations, kinking and grain pushout and pullouts [50–52] is observed, as shown at the top right corner of Fig. 9(a). These mechanisms dissipate energy in the process and lead to confinement of damage around the indentation leading to the high damage tolerance of MAX phases [47,50]. The crack which initiated at the bottom edge of the indent propagates through Ti_3SiC_2 and terminates at the interface, as shown in high magnification image in Fig. 9(b).

When the indent is oriented such that its diagonal lies along the interface between the two phases, some corner cracks that propagate along the interface are observed. For example, Fig. 10 shows an indent obtained at a test load of 0.3 kg in the NiTi–Ti_3SiC_2 interface for the bonding condition of 1000 °C, 1 h. A large (~60 μm) crack initiates very close to the NiTi–Ti_3SiC_2 interface and propagates between Ti_3SiC_2 and interfacial reaction layer, and partially through Ti_3SiC_2. Some damage in the form of delamination is observed near the corners and edges of the indent on the Ti_3SiC_2 side. Fig. 10(b) shows a BSE image of the area marked as "Area A" in Fig. 10(a). Apart from the large crack, small cracks and crack patterns are also observed in the NiTi–Ti_3SiC_2 interface. These sub-cracks branch from the large crack in Ti_3SiC_2 and stop at the interface as depicted in Fig. 10(c) which shows a high magnification BSE image of the zigzag crack pattern obtained in the interface. The zigzag crack pattern and crack branching in the interface (Fig. 10c) is unlike straight crack paths commonly observed in typical brittle materials. The common phenomena of cracks originating elsewhere and terminating at the interface, as well as their torturous propagation path in the interface suggests the formation of a strong interface between bulk NiTi and Ti_3SiC_2 components at these temperatures, regardless of the fact that interfacial reaction layer has higher hardness and, in some locations, stiffness than parent phases. Nevertheless, more quantitative testing such as interracial fracture toughness tests is needed to characterize and effectively comment on the mechanical properties of the NiTi–Ti_3SiC_2 interface.

4. Summary and conclusions

(1) Successful bonding between bulk NiTi and Ti_3SiC_2 components using solid state diffusion is realized in the temperature range of 800–1000 °C for the times of 1–10 h except at 800 °C, 1 h. Possibly, a sub-micron reaction layer forms at the interface at 800 °C after 1 h, but it is unable to withstand the thermal

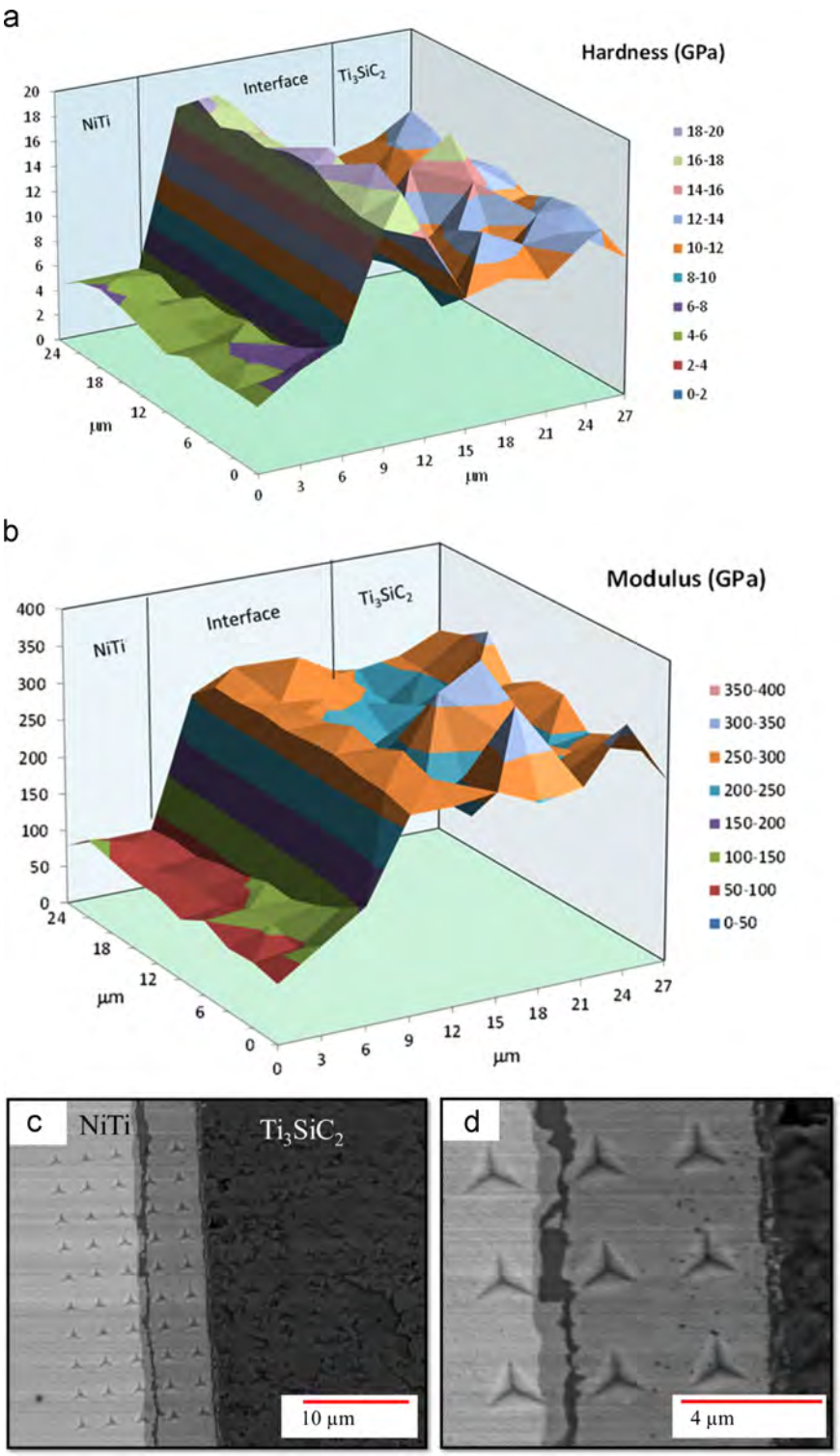

Fig. 8. 3-Dimensional plot of the (a) hardness in GPa and (b) elastic modulus in GPa, obtained using nano-indentation across the NiTi–Ti_3SiC_2 interface for the bonding condition of 1000 °C, 5 h, (c) BSE image of the locations of the indents where the plots in (a) and (b) were generated and (d) high magnification BSE image showing indents in different reaction phases.

residual stresses generated during cooling to the room temperature, leading to debonding.

(2) The reaction phases in the NiTi–Ti_3SiC_2 interface are characterized and the reaction mechanisms are proposed. Three uniform, distinct layers of Ti_2Ni, Ti_5Si_3, NiTiSi phases are formed between NiTi and Ti_3SiC_2, thus making the interfacial structure of the form NiTi/Ti_2Ni/Ti_5Si_3/NiTiSi/Ti_3SiC_2.

(3) The overall reaction layer thickness grows with a square root of the time at each temperature indicating that mechanism of solid state diffusion in the interface follows a parabolic kinetic law. Diffusion of Si into NiTi from Ti_3SiC_2 and Ni from NiTi into the reaction zone is responsible for the formation of reaction layers in the interface and thus for the bonding at these conditions. However, the rate limiting step is diffusion of Si from Ti_3SiC_2.

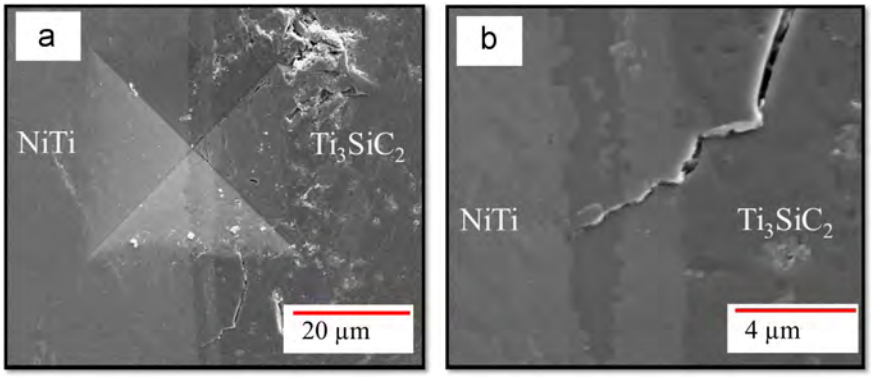

Fig. 9. (a) Secondary electron (SE) image of the indent obtained during Vickers micro-hardness tests at a load of 0.5 kg on the NiTi–Ti_3SiC_2 interface bonded at 1000 °C, 5 h, (b) high magnification SE image of the crack initiated at the bottom edge of the indent terminating at the interface shown in (a).

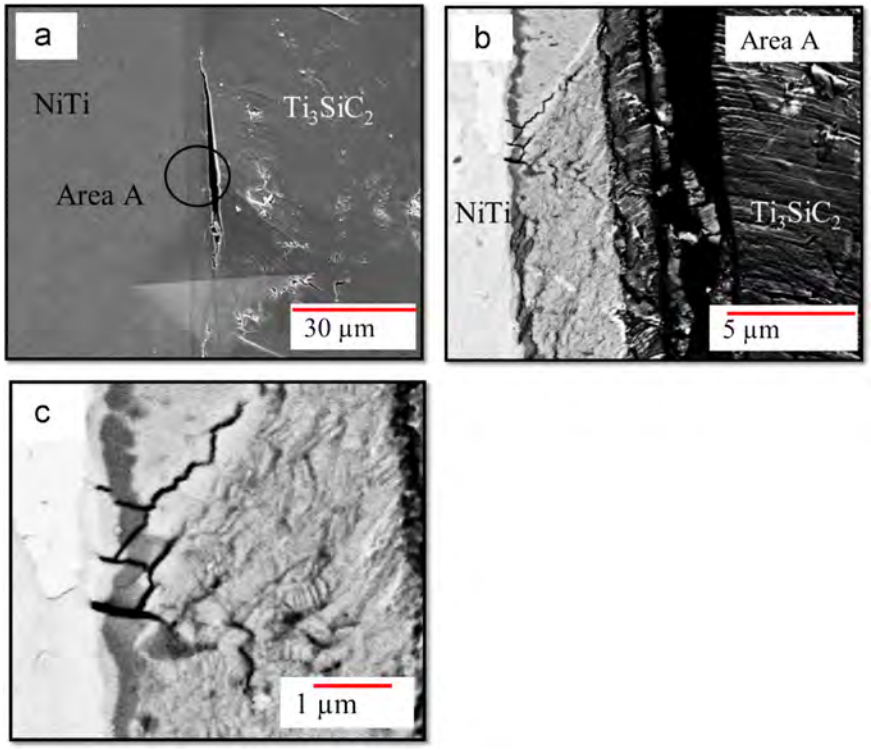

Fig. 10. (a) Secondary electron (SE) image of the indent obtained during Vickers micro-hardness tests at a load of 0.3 kg on the NiTi–Ti_3SiC_2 interface bonded at 1000 °C, 1 h, (b) backscattered electron (BSE) image of the "Area A" marked in (a), and (c) high magnification BSE image of the zigzag crack pattern obtained in the interface as shown in (b).

(4) Nano-indentation results show that the elastic moduli of the phases in the interface are higher than that of NiTi and close to that of Ti_3SiC_2. An average elastic modulus of 278.68 ± 10.02 GPa is obtained for the interface as compared to 91.62 ± 11.16 GPa for NiTi and 263.21 ± 31.89 GPa for Ti_3SiC_2. The hardness of the phases in the interface is higher than that of Ti_3SiC_2 and NiTi. An average hardness of 17.55 ± 0.95 GPa is obtained for the interface as compared to 5.44 ± 0.73 GPa for NiTi and 11.86 ± 1.80 GPa for Ti_3SiC_2.

(5) Vicker's micro-hardness tests are employed for qualitative mechanical characterization of the NiTi–Ti_3SiC_2 interface. The indents obtained by Vickers test near the interface region lead to cracks which terminate at the interface. Secondary zigzag crack patterns are also observed in the interface indicating a good resistance to the crack propagation. However, quantitative characterization such as fracture toughness measurements are needed to effectively comment on the mechanical properties of the interface.

Acknowledgments

This research was supported by the US Air Force Office of Scientific Research (AFOSR), MURI Program (FA9550-09-1-0686) to Texas A&M University, with Dr. David Stargel as the program manager. Additional support was received from the National Science Foundation under Grant no. DMR 08-44082, which supports the International Materials Institute for Multi-functional Materials for Energy Conversion (IIMEC) at Texas A&M University. The authors acknowledge the facilities, and the scientific and technical assistance, of the Australian Microscopy & Microanalysis Research Facility at the University of Sydney, especially the assistance of Dr. Patrick Trimby, in performing the EBSD analysis.

References

[1] M.W. Barsoum, M. Radovic, Encyclopedia of Materials Science and Technology, in: R.W. Cahn, et al., (Eds.), Elsevier, Amsterdam, 2004.

[2] M.W. Barsoum, Encyclopedia of Materials Science and Technology, in: R.W. Cahn, et al., (Eds.), Elsevier, Amsterdam, 2004.
[3] M.W. Barsoum, Phases: Properties of Machinable Carbides and Nitrides, Wiley VCH GmbH & Co, Germany, 2013.
[4] M. Radovic, M.W. Barsoum, Am. Ceram. Soc. Bull. 92 (2013) 20.
[5] M.W. Barsoum, T. Zhen, S.R. Kalidindi, M. Radovic, A. Murugaiah, Nat. Mater. 2 (2003) 107.
[6] M. Radovic, M.W. Barsoum, T. El-Raghy, S.M. Wiederhom, W.E. Luecke, Acta Mater. 50 (2002) 1297.
[7] M.W. Barsoum, M. Radovic, Annu. Rev. Mater. Res. 9 (41) (2013) 1.
[8] F. Barcelo, S. Doriot, T. Cozzika, M. Le Flem, J.L. Béchade, M. Radovic, M.W. Barsoum, J. Alloy. Compd. 488 (2009) 181.
[9] M. Radovic, M.W. Barsoum, T. El-Raghy, S. Wiederhorn, J. Alloy. Compd. 361 (2003) 299.
[10] Y. Zhang, Z. Sun, Y. Zhou, Mater. Res. Innovat. 3 (1999) 80.
[11] Y.C. Zhou, B.Q. Chen, X.H. Wang, C.K. Yan, Mater. Sci. Technol. 20 (2004) 661.
[12] Z. Zhang, S. Xu, Rare Met. 26 (2007) 359.
[13] W.J. Wang, V. Gauthier-Brunet, G.P. Bei, G. Laplanche, J. Bonneville, A. Joulain, S. Dubois, Mater. Sci. Eng. A 530 (2011) 168.
[14] H. Li, L.M. Peng, M. Gong, L.H. He, J.H. Zhao, Y.F. Zhang, Mater Lett. 59 (2005) 2647.
[15] S. Amini, M.W. Barsoum, Mater. Sci. Eng. A 527 (2010) 3707.
[16] A. Kothalkar, R. Benitez, L. Hu, M. Radovic, I. Karaman, Metall. Mater. Trans. A 45 (2014) 1.
[17] L. Hu, A. Kothalkar, G. Proust, I. Karaman, M. Radovic, J. Alloy. Compd. 610 (2014) 635.
[18] T. Duerig, A. Pelton, D. Stockel, Mater. Sci. Eng. A 149 (1999) 273–275.
[19] Jan Van Humbeeck, Mater. Sci. Eng. A 273–275 (1999) 134.
[20] J. Ma, I. Karaman, R.D. Noebe, Int. Mater. Rev. 55 (2010) 257.
[21] B. Lester, A. Kothalkar, M. Radovic, I. Karaman, D. Lagoudas, Composites B, 2014, in review.
[22] S. Basu, M.F. Ozaydin, A. Kothalkar, I. Karaman, M. Radovic, Scr. Mater. 65 (2011) 237.
[23] E.T.F. Chau, C.M. Friend, D.M. Allen, J. Hora, J.R. Webster, Mater. Sci. Eng. A 589 (2006) 438–440.
[24] G.R. Mirshekari, A. Saatchi, A. Kermanpur, S.K. Sadrnezhaad, Opt. Laser Technol. 54 (2013) 151.
[25] S. Fukumoto, T. Inoue, S. Mizuno, K. Okita, T. Tomita, A. Yamamoto, Sci. Technol. Weld. Join. 15 (2010) 124.
[26] X.M. Qiu, M.G. Li, D.Q. Sun, W.H. Liu, J. Mater. Process. Technol. 176 (2006) 8.
[27] H. Gugel, A. Schuermann, W. Teisen, Mater. Sci. Eng. A 668 (2008) 481–482.
[28] J. Vannod, M. Bornert, J.-E. Bidaux, L. Bataillard, A. Karimi, J.-M. Drezet, M. Rappaz, A. Hessler-Wyser, Acta Mater. 59 (2011) 6538.
[29] L. Quintino, L. Liu, R.M. Miranda, R.J.C. Silva, A. Hub, Y. Zhou, Mater. Lett. 98 (2013) 142.
[30] T.W. Clyne, P.J. Withers, An Introduction to Metal Matrix Composites, first ed., Cambridge University Press, Cambridge, 1993.
[31] M.G. Nicholas, Joining Processes, Kluwer Academic Publishers, The Netherlands, 1998.
[32] Y. Du, C. He, J.C. Schuster, S. Liu, H. Xu, Int. J. Mater. Res. 97 (2006) 543.
[33] Materials – The Landolt–Börnstein Database, in: N. Lebrun, G. Effenberg, S. Ilyenko (Eds.), Springer, Germany, 2006.
[34] Y. Zhou, Z.J. Sun, Phys. Condens. Matter 12 (2000) L457.
[35] W.L. Gu, Y.C. Zhou, Trans. Nonferrous Met. Soc. China 16 (2006) 1281.
[36] O. Dezellus, R. Voytovych, A.P.H. Li, G. Constantin, F. Bosselet, J.C. Viala, J. Mater. Sci. 45 (2010) 2080.
[37] T. El-Raghy, M.W. Barsoum, M. Sika, Mater. Sci. Eng. A 298 (2001) 174.
[38] W.L. Gu, C.K. Yan, Y.C. Zhou, Scr. Mater. 49 (2003) 1075.
[39] T.L. Ngai, W. Zheng, C. Hu, H. Xie, Y. Li, Adv. Mater. Res. 211-212 (2011) 1051.
[40] X.H. Yin, M.S. Li, Y.C. Zhou, J. Mater. Res. 21 (2006) 2415.
[41] N.F. Gao, Y. Miyamoto, J. Mater. Res. 17 (2002) 52.
[42] T. El-Raghy, M.W. Barsoum, J. Appl. Phys. 83 (1998) 112.
[43] W.C. Oliver, G.M. Pharr, J. Mater. Res. 19 (2004) 3.
[44] S. Rajagopalan, A.L. Little, M.A.M. Bourke, R. Vaidyanathan, Appl. Phys. Lett. 86 (2005) 1.
[45] N.F. Gao, Y. Miyamoto, D. Zhang, J. Mater. Sci. 34 (1999) 4385.
[46] B.J. Kooi, R.J. Poppen, N.J.M. Carvalho, J.Th.M. Barsoum, M.W. Barsoum, Acta Mater. 51 (2003) 2859.
[47] M.W. Barsoum, M. Radovic, Annu. Rev. Mater. Res. 41 (2011) 195.
[48] R. Pampuch, J. Lis, L. Stobierski, M. Tymkiewicz, J. Eur. Ceram. Soc. 5 (1989) 283.
[49] M.W. Barsoum, T. El-Raghy, J. Am. Ceram. Soc. 79 (1996) 1953.
[50] T. El-Raghy, A. Zavaliangos, M.W. Barsoum, S.R. Kalidindi, J. Am. Ceram. Soc. 80 (1997) 513.
[51] A. Procopio, M.W. Barsoum, T. El-Raghy, Metall. Mater. Trans. A 31 (2000) 333.
[52] N. Tzenov, M.W. Barsoum, J. Am. Ceram. Soc. 83 (2000) 801.